Journal of Biomedical Optics

BiomedicalOptics.SPIEDigitalLibrary.org

Spectrally encoded slit confocal microscopy using a wavelength-swept laser

Soocheol Kim
Jaehyun Hwang
Jung Heo
Suho Ryu
Donghak Lee
Sang-Hoon Kim
Seung Jae Oh
Chulmin Joo

SPIE.

Spectrally encoded slit confocal microscopy using a wavelength-swept laser

Soocheol Kim,[a,†] Jaehyun Hwang,[a,†] Jung Heo,[a] Suho Ryu,[a] Donghak Lee,[a] Sang-Hoon Kim,[b] Seung Jae Oh,[b] and Chulmin Joo[a,*]
[a]Yonsei University, School of Mechanical Engineering, Seoul 120-749, Republic of Korea
[b]Yonsei University, YUHS-KRIBB Medical Convergence Research Institute, Severance Biomedical Science Institute, and Department of Radiology, Seoul 120-749, Republic of Korea

Abstract. We present an implementation of spectrally encoded slit confocal microscopy. The method employs a rapid wavelength-swept laser as the light source and illuminates a specimen with a line focus that scans through the specimen as the wavelength sweeps. The reflected light from the specimen is imaged with a stationary line scan camera, in which the finite pixel height serves as a slit aperture. This scanner-free operation enables a simple and cost-effective implementation in a small form factor, while allowing for the three-dimensional imaging of biological samples. [DOI: 10.1117/1.JBO.20.3.036016]

Keywords: microscopy; confocal microscopy; three-dimensional microscopy; spectrally encoded confocal microscopy.
Paper 140684RR received Oct. 23, 2014; accepted for publication Mar. 10, 2015; published online Mar. 26, 2015.

1 Introduction

Confocal reflectance microscopy (CRM) provides high-resolution, three-dimensional (3-D) images of materials and biological specimens.[1,2] In general, an image in CRM is formed by serial acquisition of back-reflected light from a specimen, while a focused beam scans through the sample in three dimensions. The depth sectioning of CRM is enabled by a physical pinhole in the detection path, which allows light from the focus to pass through while rejecting the out-of-focus light. Although this point-by-point scanning approach enables high-resolution confocal imaging, the image acquisition speed is inherently limited by the mechanical scanning of the probe beam or sample, along with its serial signal acquisition. Commercial high-speed confocal microscopes thus employ expensive, high-speed scanners such as acousto-optic deflectors,[3] polygon mirrors,[4,5] and resonant scanners.[6] Imaging techniques that use multiple foci or focused lines have also been demonstrated. For example, confocal microscopy based on a scanning Nipkow disc generates multiple foci with a microlens array and detects the light from the specimen with a high-sensitivity two-dimensional (2-D) image sensor.[7] This method, however, is costly to implement and requires a complicated optical arrangement. For line-scanning confocal microscopy, a specimen is illuminated by a focused line of a probe beam, and the back-reflected light is measured by a high-sensitivity sensor as either the probe beam or the sample is scanned along a single dimension.[3]

Spectrally encoded confocal microscopy (SECM) represents one of the strategies for high-speed confocal microscopy.[8,9] In SECM, the spatial information along one direction is encoded by the wavelengths, and spectrally resolved measurement of the reflected light enables the acquisition of spatial information along that direction. Therefore, beam scanning in the slow axis only is required to obtain images. SECM has been demonstrated with spectrometers and wavelength-swept lasers.[10,11] Eliminating the entire beam scanning process would make its implementation simpler and further enhance the imaging speed. Spectrally encoded slit confocal microscopy (SESCoM) was developed to enable scanless SECM imaging.[12] This method employed a high-power broadband light source and a bulky 2-D imaging spectrometer to illuminate the specimen with multiple spectral lines and to perform spectrally resolved detection of those lines.

Here, we present another strategy for SESCoM using a wavelength-swept light source. SESCoM implementation based on a sweep source (SESCoM-SS) enables simpler and efficient imaging, which can potentially be transformed into a handheld confocal imaging probe. In operation, light from a swept source is focused into a line on a specimen via a diffraction grating and objective. As the diffraction angle varies with wavelength, the illumination line scans over the specimen as the wavelength sweeps. The reflected light from the specimen is then imaged with a stationary line scan camera (LSC). Acquisition of the line images during a single sweep of the laser generates a 2-D image of the sample without any mechanical scanning of probe beam or sample. Furthermore, the finite pixel height of the LSC is exploited as a slit aperture to enable depth-resolved imaging. This approach is particularly attractive in implementation of handheld confocal microscopy, which is useful in skin and oral tissue imaging *in vivo*.[13,14] We demonstrate the high-contrast, 3-D imaging capability of SESCoM-SS by presenting the images of various samples acquired at 83 fps.

2 Spectrally Encoded Slit Confocal Microscopy Swept Source Setup

A SESCoM-SS prototype is illustrated in Fig. 1. For demonstration, we used a custom-built wavelength-swept light source consisting of a white-light source (Fianium Ltd., SC400, UK) and a wavelength tuning filter based on a diffraction grating and a

*Address all correspondence to: Chulmin Joo, E-mail: cjoo@yonsei.ac.kr

†Authors contributed equally.

1083-3668/2015/$25.00 © 2015 SPIE

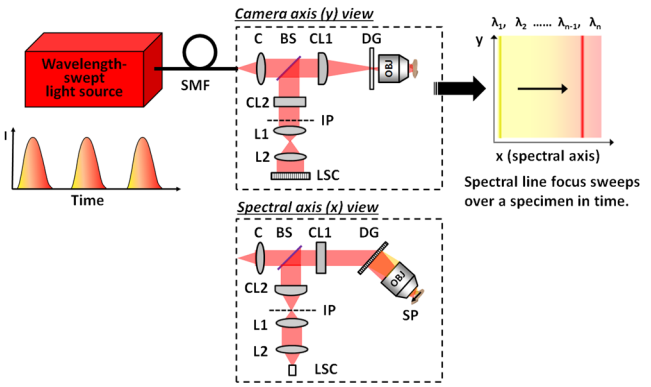

Fig. 1 Schematic of spectrally encoded slit confocal microscopy swept source (SESCoM-SS). Light from a wavelength-swept light source is focused in a line via a cylindrical lens (CL1) on a diffraction grating (DG). The light is then diffracted as a function of wavelength along the spectral axis and focused into a line over a specimen with an objective (OBJ). The line focus is scanned through a specimen as the wavelength sweeps in time. The light scattered from the specimen is collected by the same objective and subsequently imaged by a line scan camera (LSC). The telescope composed of L1 and L2 is employed to fully utilize the pixel array of the LSC. The finite pixel height of the LSC serves as a slit aperture for depth sectioning. C: collimator; BS: beamsplitter; DG: diffraction grating; SMF: single-mode fiber; CL1-CL2: cylindrical lenses; IP: intermediate image plane, L1-L2: spherical lenses, OBJ: objective; LSC: line scan camera.

galvanometer mirror. However, it should be noted that commercially available compact wavelength-swept lasers can be employed. The light source generated light centered at 700 nm with a wavelength tuning range of 600 to 800 nm. The light from the source was delivered to the SESCoM-SS imaging probe through a single-mode fiber (SMF; Thorlabs Inc., P3-630A-FC-1).

In the probe arm, the light from the fiber was collimated with a diameter of ~8.8 mm by an achromatic doublet (Thorlabs Inc., $f = 40$ mm, AC254-040-B). The light was then focused into a line on a diffraction grating (Wasatch Photonics, Inc., 600 lines/mm, 1006-1) with a cylindrical lens (CL1; Thorlabs Inc., $f = 100$ mm, ACY254-100-B), diffracted by the grating along the spectral axis (i.e., x-axis), and subsequently focused into a line on a specimen via the objective (Nikon $40\times/0.75$, Japan). The backscattered light from the specimen was collected by the same objective and imaged onto an intermediate image plane (IP) via a CL2 (Thorlabs Inc., $f = 50$ mm, ACY254-050-B). The image was further magnified by a telescope composed of L1 and L2 by a factor of 2.86 prior to the LSC. This telescope was employed to fully utilize the pixel array in the LSC. The magnification ratios in the spectral (x) and camera (y) axes were ~28 and ~57, respectively. The LSC (2048 pixels, 14 μm × 14 μm, e2v, AVIIVA EM4, UK) acquired the line image at 50 kHz. For the employed light source with $\Delta\lambda = 200$ nm, we found that the diffraction angle from the grating (θ_x) varied from 8.6 deg to 15.6 deg at the back focal plane of the objective. The field-of-view in the spectral axis (FOV_x) can thus be estimated as $\mathrm{FOV}_x = 2f_{\mathrm{OBJ}}\tan(\theta_x/2) \sim 611$ μm, with the objective focal length, f_{OBJ}. The FOV along the camera axis (i.e., y-axis), on the other hand, can be estimated by $\mathrm{FOV}_y = 2f_{\mathrm{OBJ}}\tan(\theta_y/2)$, where θ_y is the diverging angle of the light at the back focal plane of the objective along the y-axis. It was found to be ~440 μm.

3 Results

3.1 *SESCoM-SS Lateral Resolutions*

The lateral resolutions of SESCoM-SS should be considered differently in each axis. The resolution in the camera axis (i.e., y-axis) is mainly determined by the NA of the imaging optics as a result of the full-field illumination along the direction. The diffraction-limited FWHM lateral resolution can be estimated by $0.51 \times \lambda/\mathrm{NA}$ (Ref. 15) as in a conventional microscope, which yields ~0.48 μm.

The resolution in the spectral (x) axis, on the other hand, is determined by the element with the poorest resolution between the values governed by the effective spectral resolution and the slit confocal setup in the SESCoM-SS. We first examine the lateral resolution governed by the effective spectral resolution. As noted in Ref. 11, the spectral resolution is determined by the larger of instantaneous linewidth of the light source or the spectral resolution of the grating. The spectral resolution set by the diffraction grating ($\delta\lambda_{\mathrm{G}}$) is given by[10,11]

$$\delta\lambda_{\mathrm{G}} = \frac{\lambda_0\Lambda}{D}, \tag{1}$$

where λ_0 is the center wavelength of the light source, Λ is the grating period, and D is the incident beam diameter along the grating. Using Eq. (1), we consider the beam size along the grating, since the light is diffracted by each grating line and spectrally dispersed along that direction. Evaluation of Eq. (1) with the parameters in the SESCoM-SS setup ($\lambda_0 = 0.7$ μm, $\Lambda = 1/600$ mm/lps, $D \sim 8.8$ mm) resulted in 0.133 nm. Comparing this value with the instantaneous linewidth of the light source (~0.29 nm, measured by an optical spectrometer), it is evident that the effective spectral resolution in our case is set by the instantaneous linewidth of the source. The lateral resolution determined by this spectral resolution can then be obtained as $\delta x = \mathrm{FOV}_x \times (\delta\lambda/\Delta\lambda)$.[11] Here, $\delta\lambda$ is the FWHM spectral resolution, and $\Delta\lambda$ is the tuning range of the light source. Using the parameters in our setup ($\mathrm{FOV}_x = 611$ μm, $\delta\lambda = 0.29$ nm, and $\Delta\lambda = 200$ nm), the lateral resolution governed by the SESCoM-SS spectral resolution was measured to be ~0.89 μm.

We then estimate the lateral resolution set by the slit confocal arrangement in SESCoM-SS. It has been understood that the lateral response of a slit confocal microscope is similar to that of a pinhole-based confocal microscope in the slit axis, but it is the same as a conventional microscope in the other axis.[16] Hence, the lateral resolution in the slit axis can be estimated as the lateral resolution of a confocal microscope with its pinhole diameter equal to the slit width. Reference 16 provides a means to estimate the theoretical lateral resolution for a given aperture size on a specimen plane in the optical unit. The effective slit size on the specimen plane could be obtained by projecting the 14-μm slit in the detector plane onto the sample plane through the SESCoM-SS imaging optics. A simple calculation found the slit width on the sample plane to be 0.5 μm at the center wavelength (i.e., 700 nm). The half width of this slit corresponds to ~1.7 in the lateral optical unit.[1] Using this value, the half of the FWHM lateral resolution ($v_{1/2}$ with the same notation in Ref. 16) was found to be 1.28 in the optical unit, which corresponds to the FWHM lateral resolution of 0.38 μm.

We now compare the lateral resolutions determined by the effective spectral resolution and the slit confocal setup in the

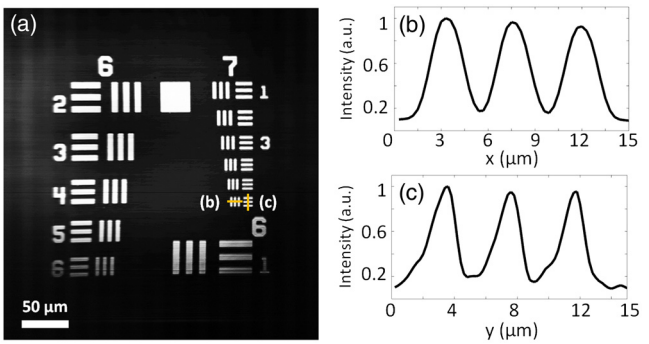

Fig. 2 (a) SESCoM-SS image of a USAF resolution target. The scale bar represents 50 μm. (b) and (c) show the intensity profiles along the lines indicated in (a).

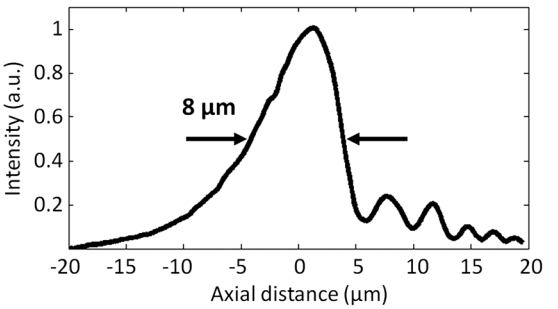

Fig. 3 Measured axial response of the SESCoM-SS setup.

SESCoM-SS. Since the lateral resolution is determined by the larger value between the estimations from the effective spectral resolution and slit confocal system, it can be concluded that the lateral resolution in the spectral axis is 0.89 μm.

We experimentally measured the lateral resolutions of SESCoM-SS by imaging a 1951 USAF resolution target (Thorlabs Inc., R1DS1P). Figure 2(a) shows the SESCoM-SS image of the target. The smallest features in groups 6 and 7 could be clearly discerned. Figures 2(b) and 2(c) show the intensity profiles along the lines indicated in Fig. 2(a). The spatial frequency of the lines of elements 6 in group 7 is 228 lps/mm. We evaluated the FWHMs of their first-order derivatives. The measured lateral resolutions were found to be 1.24 and 0.84 μm in the horizontal (spectral) and vertical directions, respectively. The differences between the estimated and measured resolutions in the x and y axes were ~0.35 and 0.46 μm, respectively.

3.2 *SESCoM-SS Axial Resolution*

Depth responses of the slit confocal microscopes have been extensively studied elsewhere.[15–17] Referring to Fig. 3.18 in Ref. 16 and the effective half width of the slit of ~1.7 in the lateral optical unit, we found that the half width of the axial response ($u_{1/2}$ using the same notation in Ref. 16) was ~3.7 in the axial optical unit. An approximate expression for the FWHM axial resolution can then be derived as

$$\delta z = 0.6\frac{\lambda_0}{n - \sqrt{n^2 - \mathrm{NA}^2}}. \quad (2)$$

The evaluation of Eq. (2) yields the theoretical FWHM axial resolution of 1.24 μm.

We experimentally assessed the axial response of our SESCoM-SS setup by acquiring the images as a planar mirror in the sample plane scanned through the focus. Figure 3 shows the measured axial response obtained by averaging the values of 3×3 pixels at the center of the FOV. The measured FWHM resolution was found to be ~8.0 μm, which is substantially larger than the theoretical estimation.

The discrepancies between the theoretical and measured resolutions may be partly accounted for by the tilt of the line focus produced by the CL1 with respect to the grating plane. The line focus was incident on the diffraction grating with an angle of ~14 deg, therefore, the focal shifts along the grating lines could lead to a wavefront distortion at the back focal plane of the objective. Moreover, our analysis with ZEMAX software found that the chromatic and spherical aberrations of CL1 produce focal shifts of up to ~370 and ~10 μm, respectively. These may also lead to the degradation of spatial resolutions.

3.3 *SESCoM-SS Biological Imaging*

The biological imaging capability of SESCoM-SS was assessed by imaging various biological specimens. Figure 4 shows the representative SESCoM-SS images of the excised liver tissue of a cow recorded at different locations. It can be noted that distinctive structural arrangements could be observed at the different locations. Previous CRM imaging studies on liver tissues indicate that the hepatocytes could be identified as moderately refractile structures with the nucleus appearing as a centered hyporefractile spot (dark spot on the images).[18] Our SESCoM-SS images could also visualize the hepatocytes, as indicated by the arrows in Figs. 4(a) and 4(b). The insets show the magnified views of the hepatocytes identified by the SESCoM-SS. A different morphology can be seen in Fig. 4(c), where the portal vein was indicated by the arrowhead.

The depth-sectioning capability of our SESCoM-SS setup was further tested by acquiring images of an excised mouse cardiac tissue. We performed SESCoM-SS imaging while the sample was scanned along the optical axis. The representative images at the tissue surface and in ~10 μm steps below the surface are shown in Fig. 5. An intricate network of cellular structures, which may include myocytes and myofibroblasts, could be visualized with high contrast. All the images were acquired at 83 fps.

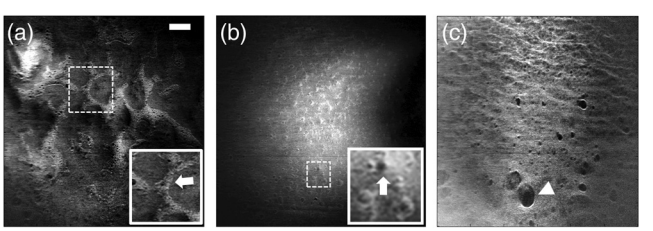

Fig. 4 Representative SESCoM-SS images of excised liver tissue of a cow. (a)–(c) show the images acquired at different locations in the sample. The insets in (a) and (b) show the magnified views of the regions marked with dashed rectangles. The hepatocytes are indicated by the arrows. The arrowhead in (c) indicates a vein in the liver tissue. The scale bar represents 50 μm.

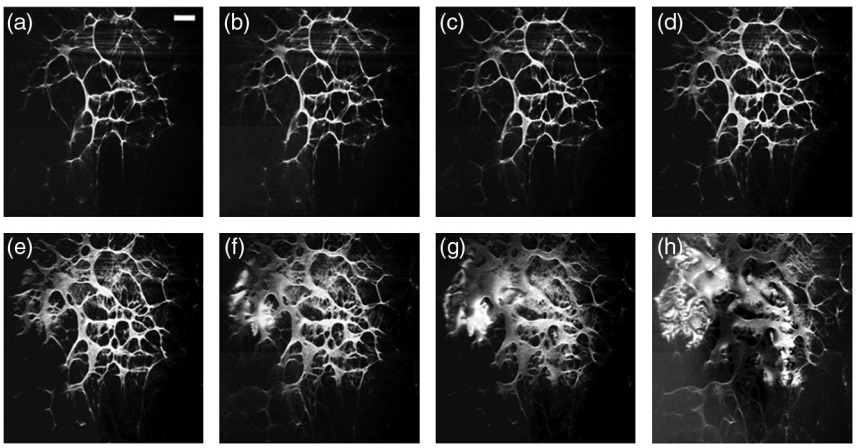

Fig. 5 Depth-resolved SESCoM-SS images of an excised mouse cardiac tissue. (a)–(h) show the images acquired at 10-μm steps in depth. The intricate cellular networks were visualized with high contrast. The scale bar denotes 50 μm.

4 Discussion

A notable feature of SESCoM-SS lies in its simplicity of implementation and operation. As the SESCoM-SS probe does not require a dedicated beam scanner, physical slit aperture, and complicated optical arrangement, it allows compact and cost-effective implementation. In the previous SESCoM setup,[12] a specimen was simultaneously illuminated with multiple spectral lines, and the coordinates in the sample were mapped into both wavelengths and one-dimensional coordinates. The light scattered from the sample was recombined at a diffraction grating, passed through a physical slit aperture, and then spectrally dispersed again by another grating to be imaged with a high-sensitivity 2-D image sensor. This configuration required two diffraction gratings in the detection path and more optical elements, making the system bulky and inefficient. In contrast, for our SESCoM-SS, the sample is illuminated by a line focus of a specific wavelength at a given time. Therefore, the backscattered light from the specimen is diffracted by the diffraction grating just once and is directly measured by an LSC. The finite pixel height of the LSC serves as a slit aperture, alleviating the need for a physical aperture and the alignment of the slit relative to the camera pixel array. It should be noted, though, that the external slit apertures may be employed to further enhance spatial resolution. The SESCoM-SS involves a smaller number of diffraction gratings and optical elements, which makes it more advantageous in probe miniaturization and signal detection efficiency.

The lateral resolutions in SESCoM-SS were determined differently in each axis. In our prototype, the lateral resolution in the y-axis was governed by the NA of the imaging optics, whereas the resolution in the spectral axis was mainly determined by the instantaneous linewidth of the light source. Even though the slit confocal imaging based on the finite pixel height of the LSC provided higher spatial resolution ($\sim$0.36 μm), the instantaneous linewidth of 0.29 nm of the light source led to the actual measured resolution of $\sim$1.24 μm. Improvement in the spatial resolution can be readily achieved by replacing the light source with other types of wavelength-swept lasers with a smaller linewidth. For example, high-speed, compact wavelength-swept lasers based on microelectromechanical systems (MEMS) tunable filters are commercially available with a linewidth of <0.1 nm. Even faster wavelength sweeps are possible with recent advances in fiber-based swept lasers.

Our method, a type of line-scanning confocal microscopy, may not outperform other point-scanning confocal microscopes.[16] It has been known that the line-confocal imaging systems exhibit thicker axial resolution compared with the point-scanning systems.[17] The use of LSC may also hinder its implementation into a small endoscope. However, its simple, scanner-free operation, along with the demonstrated depth-resolved imaging capability for biological samples make it a promising candidate for small handheld confocal imaging systems. Handheld confocal scanners have been implemented with miniaturized MEMS-based scanners inside the probe.[13,19] Yet, the MEMS-based scanners suffer from mechanical and electrical issues including fatigue, fracture, electrostatic interference, and dielectric breakdown.[20,21] The scanner-free operation of our method is, therefore, highly attractive in terms of probe implementation and reliability. Future development of this microscope may involve implementation of the SESCoM-SS probe in a portable form, with potential applications in *in vivo* skin and oral tissue imaging as well as an imaging tool in open surgical settings.[13,14]

Acknowledgments

This research was supported by the research programs of National Research Foundation of Korea (NRF) (NRF-2012R1A1A1003867) and by the Korean Health Technology Research and Development Project of the Ministry for Health, Welfare and Family Affairs (HI10C19110300).

References

1. J. Pawley, *Handbook of Biological Confocal Microscopy*, Springer, New York (2010).
2. S. W. Paddock, "Confocal laser scanning microscopy," *Biotechniques* **27**(5), 992–1007 (1999).
3. K.-B. Im et al., "Simple high-speed confocal line-scanning microscope," *Opt. Express* **13**(13), 5151–5156 (2005).
4. S. Choi et al., "Development of a high speed laser scanning confocal microscope with an acquisition rate up to 200 frames per second," *Opt. Express* **21**(20), 23611–23618 (2013).
5. K. H. Kim, C. Buehler, and P. T. So, "High-speed, two-photon scanning microscope," *Appl. Opt.* **38**(28), 6004–6009 (1999).

6. T. Collier et al., "Near real-time confocal microscopy of amelanotic tissue: detection of dysplasia in *ex vivo* cervical tissue," *Acad. Radiol.* **9**(5), 504–512 (2002).
7. T. Tanaami et al., "High-speed 1-frame/ms scanning confocal microscope with a microlens and Nipkow disks," *Appl. Opt.* **41**(22), 4704–4708 (2002).
8. G. J. Tearney, R. Webb, and B. Bouma, "Spectrally encoded confocal microscopy," *Opt. Lett.* **23**(15), 1152–1154 (1998).
9. D. Kang et al., "Endoscopic probe optics for spectrally encoded confocal microscopy," *Biomed. Opt. Express* **4**(10), 1925–1936 (2013).
10. D. Yelin et al., "Large area confocal microscopy," *Opt. Lett.* **32**(9), 1102–1104 (2007).
11. C. Boudoux et al., "Rapid wavelength-swept spectrally encoded confocal microscopy," *Opt. Express* **13**(20), 8214–8221 (2005).
12. J. Kim, D. Kang, and D. Gweon, "Spectrally encoded slit confocal microscopy," *Opt. Lett.* **31**(11), 1687–1689 (2006).
13. C. L. Arrasmith, D. L. Dickensheets, and A. Mahadevan-Jansen, "MEMS-based handheld confocal microscope for *in-vivo* skin imaging," *Opt. Express* **18**(4), 3805–3819 (2010).
14. Y. Wang et al., "Portable oral cancer detection using a miniature confocal imaging probe with a large field of view," *J. Micromech. Microeng.* **22**(6), 065001 (2012).
15. T. R. Corle, C.-H. Chou, and G. S. Kino, "Depth response of confocal optical microscopes," *Opt. Lett.* **11**, 770–772 (1986).
16. T. Wilson, *Confocal Microscopy*, Academic Press, London (1990).
17. C. Sheppard and X. Mao, "Confocal microscopes with slit apertures," *J. Mod. Opt.* **35**(7), 1169–1185 (1988).
18. V. Campo-Ruiz et al., "*In vivo* and *ex vivo* virtual biopsy of the liver with near-infrared, reflectance confocal microscopy," *Mod. Pathol.* **18**(2), 290–300 (2004).
19. H.-J. Shin et al., "Fiber-optic confocal microscope using a MEMS scanner and miniature objective lens," *Opt. Express* **15**(15), 9113–9122 (2007).
20. W.-M. Zhang, G. Meng, and D. Chen, "Stability, nonlinearity and reliability of electrostatically actuated MEMS devices," *Sensors* **7**(5), 760–796 (2007).
21. S. T. Holmstrom, U. Baran, and H. Urey, "MEMS laser scanners: a review" *J. Microelectromech. Sys.* **23**(2), 259–275 (2014).

Biographies of the authors are not available.